Active Anticorrosion Coatings with Halloysite Nanocontainers

Dmitry G. Shchukin,*,† S. V. Lamaka,‡ K. A. Yasakau,‡ M. L. Zheludkevich,‡ M. G. S. Ferreira,‡,§ and H. Möhwald†

Max-Planck Institute of Colloids and Interfaces, D14476 Golm, Germany, University of Aveiro, CICECO, Department of Ceramics and Glass Engineering, 3810-193, Aveiro, Portugal, and Instituto Superior Técnico, Department of Chemical Engineering, Avenue Rovisco Pais 1049-001, Lisboa, Portugal

Received: August 2, 2007; In Final Form: November 6, 2007

This work contributes to the development of a new generation of active corrosion protection coatings composed of hybrid sol−gel films doped with halloysite nanotubes able to release entrapped corrosion inhibitors in a controllable way. A silica-zirconia-based hybrid film was used in this work as an anticorrosion coating deposited on 2024 aluminum alloy. Halloysite nanotubes with inner voids loaded by corrosion inhibitors (2-mercaptobenzothiazole) and outer surfaces layer-by-layer covered with polyelectrolyte multilayers were introduced into the hybrid films. The sol−gel film with the nanocontainers reveals enhanced long-term corrosion protection in comparison with the undoped sol−gel film. This effect is obtained because of the self-controlled release of the corrosion inhibitor triggered by the corrosion processes. Utilization of the inner halloysite nanotube lumen as a storage medium for the corrosion inhibitor offers a novel way of fabricating composite core−shell type nanomaterials with their further application as a main component of feedback-active coatings.

Introduction

Corrosion of metals is one of the main destruction processes resulting in huge economic losses, especially in the aerospace, automotive, and petroleum industries. Polymer or sol−gel coatings are normally applied on the metal surface providing a barrier for permeation of corrosive species.[1,2] However, when the barrier is damaged and the corrosive agents penetrate the metal surface the coating system cannot stop the corrosion process. So far, the most effective anticorrosion coatings for active protection of metals are chromate-containing systems.[3] The drawback of chromates is their superior oxidation properties, which make them environmentally unfriendly. The hexavalent chromium species can be responsible for several diseases including cancer,[4] which is the main reason for banning Cr^{6+}-containing anticorrosion coatings in Europe in 2007.

One of the possible solutions to achieve active corrosion protection is to introduce an environmentally friendly corrosion inhibitor directly into the coating, providing release of the inhibitor and termination of the corrosion propagation at already damaged corrosion defects. The behavior of the inhibitor directly embedded into sol−gel coatings depends on the chemical nature of each inhibitor and can lead to weakening of the protection properties of the coatings.[5] The inhibitor is effective only if its solubility and release rate in the defect environment is in the right range. Very low solubility leads to a lack of the inhibitor at the substrate interface and consequently to weak feedback activity. If the solubility is too high then the substrate will be protected, but for only a relatively short time because the inhibitor will be leached out from the coating rapidly. Another drawback, which can appear because of high solubility, is the osmotic pressure that leads to blistering and delamination of the protective coating.

Recent achievements in surface science open a new avenue for fabrication of coatings with active anticorrosion properties through the integration of nanoscale containers (carriers) loaded with the inhibitor or any other active compound into existing "passive" films, thus designing completely new coating systems based on the "passive" matrix−"active" container structure. The main idea here is to develop nanocontainers, which can be sensitive to the external (e.g., mechanical damage) or internal (e.g., pH changes) corrosion trigger.[6−8] When the local environment undergoes changes or if the corrosion process is started on the metal surface, the nanocontainers release encapsulated active material (inhibitor) directly into the damaged area thus preventing undesirable leakage of the inhibitor and reduction of the barrier properties of the film.

Up to date, there are only several reports exploring the possibility to form self-healing anticorrosion coatings based on incorporated nanocontainers. Direct deposition of the polyaniline-coated polystyrene latex particles on an iron plate increased the anticorrosion protection of the iron.[9] Polyaniline/polystyrene particles of 1.85 μm in diameter were synthesized by chemical polymerization of aniline on the polystyrene latex particles in the suspension resulting in a core−shell structure. Another example of container-based coatings are heat expandable spheres for car protection based on ethylvinylacetate derivatives.[10] White et al. demonstrated the effective application of micrometer-scale capsules loaded with oligomers for self-healing of the cracks in polymer coatings.[11,12]

Active corrosion protection can also be provided by employing mesoporous containers dispersed in a polymeric matrix material.[13] The porous container structure can be filled with either organic or inorganic inhibitors. During the operating lifetime, a progressive permeation of oxygen and water into the polymer-based coating occurs. Moreover, bifunctional anticorrosion and antifriction coatings can be designed combining inhibitors and oil-loaded containers.[14] Self-healing can be also achieved using the ion-exchange properties of the nanocontainer

* Corresponding author. E-mail: dmitry.shchukin@mpikg.mpg.de.
† Max-Planck Institute of Colloids and Interfaces.
‡ University of Aveiro.
§ Instituto Superior Técnico.

10.1021/jp076188r CCC: $40.75
Published on Web 01/09/2008 PAGE EST: 6.5

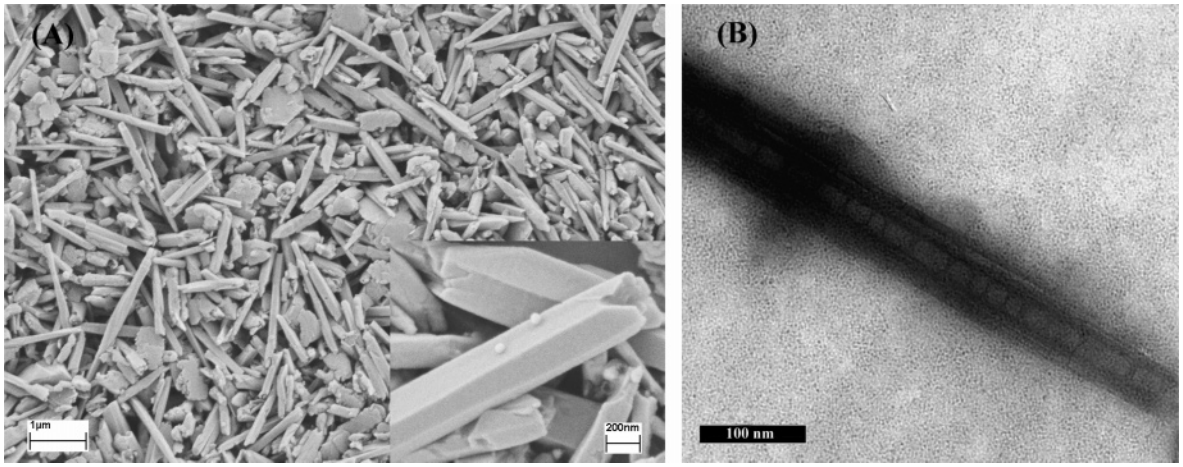

Figure 1. SEM (A) and TEM (B) images of the halloysite nanocontainers.

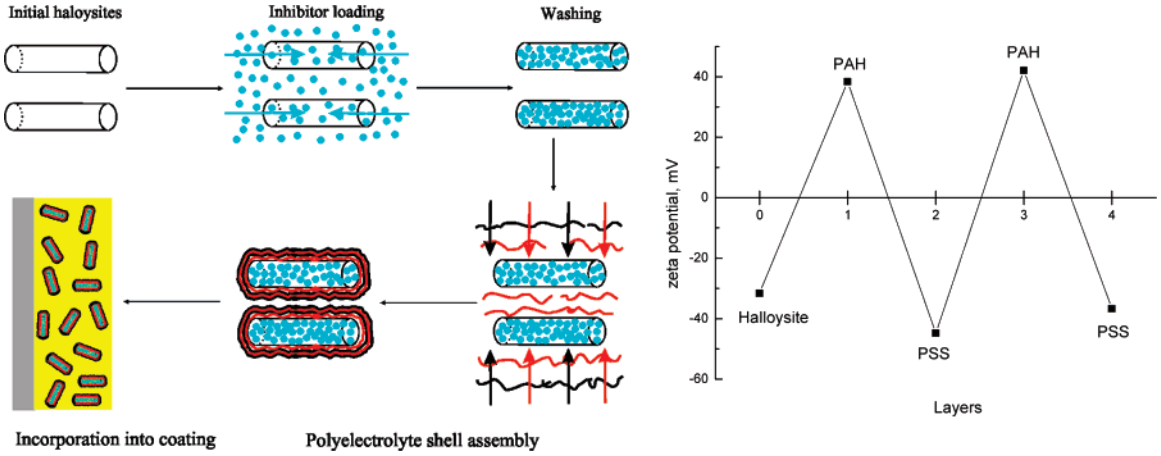

Figure 2. Left: schematic illustration of the fabrication of 2-mercaptobenzothiazole-loaded halloysite/polyelectrolyte nanocontainers. Right: zeta potential data for sequential deposition of PAH and PSS polyelectrolytes on halloysite nanotubes, pH 7.5.

core. Compositions that release corrosion-inhibiting agents from particles include ion-exchange resins, ion-exchanged zeolites, ion-exchanged solid particles, and water-soluble glasses.[15]

However, the large-scale implementation of the nanocontainer-based coatings is limited by the nanocontainer price, which is too high to make self-healing coating commercially competitive. This calls for the finding of low-cost nanocontainers, which can be employed successfully in self-healing coatings. One of the prospective future containers can be industrially mined halloysite nanotubes. Halloysite was found to be a viable and inexpensive nanoscale container ($4/kg with a supply of 50 000 tons per year) for the encapsulation of biologically active molecules that was first demonstrated by Price et al.[16] The lumen of the halloysite was used as an enzymatic nanoreactor.[17] A strong surface charge on the halloysite tubules was exploited for designing nano-organized multilayers using the layer-by-layer (LbL) method.[18,19]

Halloysite is defined as a two-layered aluminosilicate, chemically similar to kaolin, which has a predominantly hollow tubular structure in the submicrometer range.[20,21] The neighboring alumina and silica layers create a packing disorder causing them to curve. As for most natural materials, the size of halloysite particles varies within 1−15 μm of length and 10−150 nm of inner diameter depending on the deposits. The ζ potential of halloysite particles is negative at pH 6−7 and similar to the surface potential of SiO_2 with a small contribution from the positive Al_2O_3 inner surface[22] (chemical properties on the halloysite nanotubes' outermost surface are similar to the properties of SiO_2 while the properties of the inner cylinder core could be associated with Al_2O_3). However, at pH 8.5 the tube lumen has a positive surface, promoting loading by negatively charged macromolecules and preventing their adsorption on the negatively charged outer surface. Halloysite nanotubes are capable of entrapping a range of active agents (drugs,[23] nicotinamide adenine dineculeotide,[18] marine biocides[24]) within the inner lumen, as well as within void spaces in the multilayered aluminosilicate shell, followed by their retention and release. Both hydrophobic and hydrophilic agents can be embedded after appropriate pretreatment of the halloysite.[25,26]

Herein, we demonstrate the possibility of employing cheap halloysite nanotubes as prospective nanocontainers for anticorrosion coatings with active corrosion protection. Halloysite nanotubes were loaded with the corrosion inhibitor 2-mercaptobenzothiazole, which is partly soluble in water and well-soluble in ethanol or acetone, and then incorporated into ZrO_2−SiO_2 sol−gel coating. To prevent undesirable leakage of the loaded inhibitor from the halloysite interior, we modified the outer surface of the 2-mercaptobenzothiazole-loaded halloysite nanotubes by deposition of several alternating polyelectrolyte multilayers (poly(allylamine hydrochloride)/poly(styrene sulfonate)). Another functionality of the polyelectrolyte shell is to provide the release of the encapsulated inhibitor controlled by pH changes in the environment surrounding the halloysite nanotube, which will perform inhibitor release triggered by pH changes directly in the corrosion pit. The AA2024-T3 aluminum alloy was taken as a model metal substrate. Electrochemical impedance spectroscopy (EIS), scanning electron microscopy (SEM) coupled with energy dispersive X-ray spectroscopy

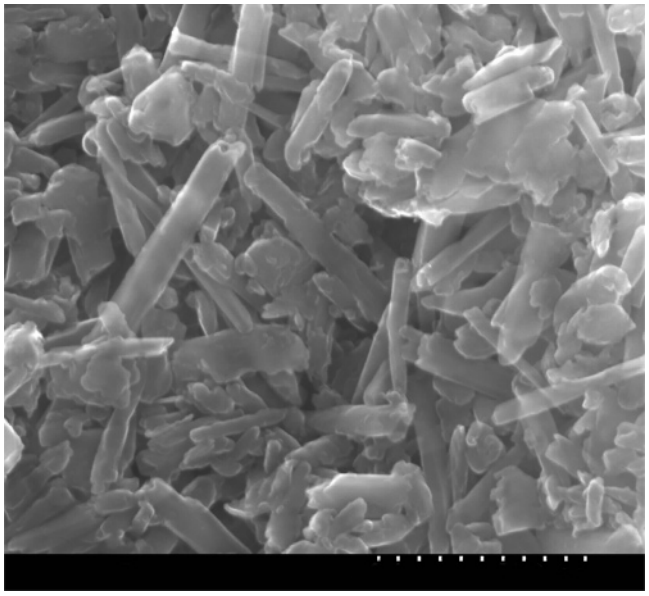

Figure 3. SEM image of halloysites doped with 2-mercaptobenzothiazole and coated with PAH/PSS/PAH/PSS polyelectrolyte layers. Scale bar is 1.5 μm.

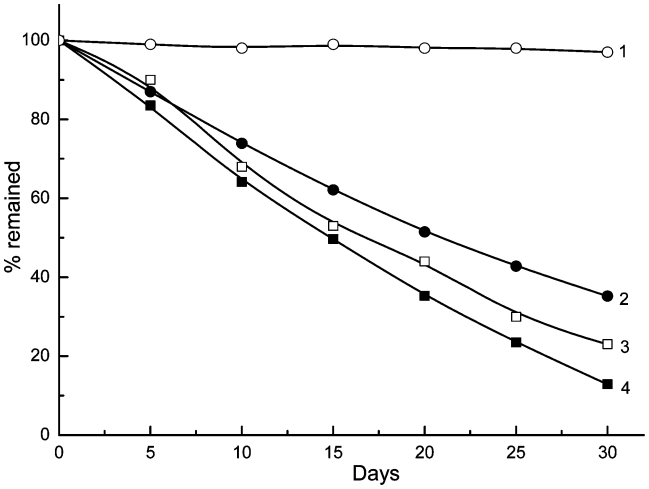

Figure 4. Release of the 2-mercaptobenzothiazole in water solution at pH = 6.5 from (1) halloysite nanotubes with PAH/PSS shell and (3) halloysite nanotubes without PAH/PSS shell; in water solution at pH = 10 from (2) halloysite nanotubes with PAH/PSS shell and (4) halloysite nanotubes without PAH/PSS shell.

(EDX), transmission electron microscopy (TEM), and atomic force microscopy (AFM) were used as the main techniques for structural and morphological characterization of sol−gel coatings and estimation of the effectiveness of anticorrosion protection.

Experimental Section

Materials. Sodium poly(styrene sulfonate) (PSS, $M_w \sim$ 70 000), poly(allylamine hydrochloride) (PAH, $M_w \sim 50\,000$), 2-mercaptobenzothiazole, HCl, zirconium (IV) n-propoxide (TPOZ), 3-glycidoxypropyltrimethoxysilane (GPTMS), propanol, ethylacetoacetate, and HNO_3 were obtained from Aldrich. Processed halloysite G was purchased from New Zealand China Clays Ltd., Auckland, New Zealand. A water suspension (10 wt %) was prepared by slow addition of water to dry halloysite and further milled in a laboratory blender to remove clay aggregates. The dispersion of the halloysite particles was improved by heating at 60 °C on a stirring hotplate for 12 h. The resulting halloysite nanotubes were separated by centrifugation, washed three times with distilled water, and dried at 60 °C in air for 12 h. Before use, dry halloysite was sieved to eliminate aggregates resulting from drying.

The 2024-T3 aluminum alloy was used in this study as a metallic substrate for the sol−gel coatings. The nominal chemical composition of the alloy is described elsewhere.[27] All panels of the alloy were chemically etched before application of the coatings. An industrial-like three-step cleaning procedure was used. Alkaline cleaning in Metaclean T2001 at 60−70 °C for 15−25 min followed by alkaline etching in Turco Liquid Aluminetch N2 at 60 ± 5 °C for 30−60 s and acid etching in Turco Liquid Smutgo NC at 30 ± 5 °C for 5−10 min were applied. Then, metallic panels were washed with distilled water.

The water used in all experiments was prepared in a three-stage Millipore Milli-Q Plus 185 purification system and had a resistivity higher than 18 MΩ·cm.

Preparation of Sol−Gel Film. The hybrid sol−gels were synthesized using a controllable sol−gel route mixing two different sols. An alkosol containing zirconia precursors was combined with an organosilane alkosol. The first sol was prepared from 70% TPOZ solution in isopropanol mixed with ethylacetoacetate at a 1:1 volume ratio. After 20 min, the synchronous ultrasonic agitation was started and water with pH 0.5 was added in stoichiometric quantity needed for TPOZ hydrolysis and condensation, which continued for 90 min. The second organosilane sol was prepared hydrolyzing GPTMS in isopropanol by addition of acidified water (pH 0.5, HNO_3) in an 8:8:1 volume ratio for 1 h under stirring. The hybrid solution was obtained by mixing the zirconium-based sol with the organosilane-based one at a 1:2 volume ratio. The final sol−gel solution was stirred under ultrasonic agitation for 1 h and then aged for 1 h. The sol−gel films were produced by dip-coating of the aluminum substrates in final sol−gel solution at a dipping/withdrawal speed of 18 cm/min and an exposition time of 100 s. Then all samples were cured at 120 °C for 80 min in air for cross-linking and gelation of sol−gel and solvent evaporation.

One of the sol−gel formulations was doped with halloysites enriched with mercaptobenzothiazole. Dry halloysites (0.04 g) were added by small portions into 0.5 mL of water and agitated ultrasonically. This suspension was introduced into the silane-based solution before hydrolysis.

Characterization. For SEM analysis, a drop of the halloysite suspension was applied to a glass wafer and dried at room temperature overnight. Then, the samples were sputtered with gold and measurements were conducted using a Gemini Leo 1550 instrument operated at 3 keV. The microstructure and general chemical composition of the sol−gel films was studied by SEM/EDX Hitachi S-4100 and Hitachi SU-70 microscopes with electron beam energies of 25 and 15 keV, respectively.

TEM images were taken from ultramicrotomed halloysite samples (slice thickness varies from 30 to 100 nm) using a Zeiss EM 912 Omega transmission electron microscope. Coated copper grids were employed to support the samples. The nanostructure of the sol−gel coating was observed by a TEM/EDS JEOL JEM 2010 microscope. The sample was prepared by gradual grinding off using a dimple grinder and ion-milling. The morphology of the sol−gel films that contain 2-mercaptobenzothiazole-loaded halloysites was assessed by an AFM (Molecular Imaging PicoSPM LE) with a Pico scan 2100 controller. The AFM was operating in tapping mode employing silicon probes with tip radii less than 10 nm.

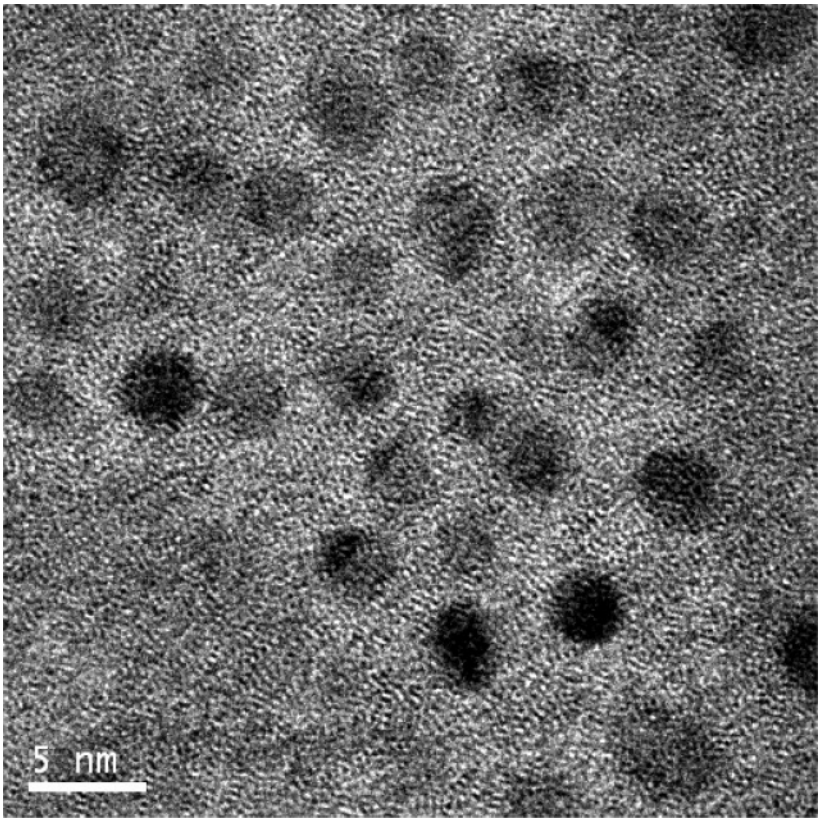

Figure 5. High-resolution TEM image of the TPOZ- and GPTMS-based sol−gel film deposited on an aluminum-based alloy and cured at 120 °C for 80 min.

The electrophoretic mobility measurements were performed using a Malvern Zetasizer 4 instrument. The quartz crystal microbalance technique (QCM, USI Systems, Japan) based on the change of the frequency of a piezoelectric crystal after deposition of additional mass was used to estimate the quantity of 2-mercaptobenzothiazole entrapped inside the inner lumen of the halloysite nanotubes. A drop of halloysite suspension (100 μL) was put onto the surface of the gold resonator and dried at 50 °C.

The EIS technique was employed to quantify the corrosion protection performance of the developed sol−gel films on aluminum alloy during immersion in 3% solution of NaCl. EIS measurements were carried out with a Gamry FAS2 Femtostat coupled with a PCI4 Controller at open circuit potential with applied 10 mV sinusoidal perturbations in the 100 kHz to 3 mHz frequency range taking 7 steps per decade. A conventional three-electrode cell was used. It is composed of a saturated calomel reference electrode, a platinum foil as a counter electrode, and sol−gel coated AA2024 substrates as working electrodes with a surface area of 3.3 cm^2. All measurements were made in a Faraday cage in order to avoid electromagnetic interference. At least two samples were measured for each coating to check the reproducibility of the results. The impedance plots were fitted using Echem Analyst software.

All measurements were carried out at ambient temperature if not differently specified.

Results and Discussion

3.1. Inhibitor-Doped Halloysites Coated with Polyelectrolyte Layers. The initial nanocarriers before loading of the 2-mercaptobenzothiazole are presented in Figure 1. Figure 1a shows an SEM image of the separated halloysite nanotubes. The initial halloysite material consists of well-defined nanotubes with sizes varying between 1 and 15 μm. The hollow lumen of the halloysite nanotubes before loading is clearly visible in Figure 1b and can be estimated as 15−40 nm in diameter. The calculated inner space provides the ability of loading 12% of the total volume of the halloysite.

Embedding of the 2-mercaptobenzothiazole inside the inner volume of the halloysite nanotubes (see overall scheme of nanocontainer fabrication in Figure 2) was performed adapting the procedure described by Price et al.[24] Dispersed halloysite powder was mixed with 10 mg/mL solution of 2-mercaptobenzothiazole in ethanol. A vial containing the mixture was transferred to a vacuum jar and then evacuated using a vacuum pump. Slight fizzing of the suspension indicates the air being removed from the halloysite interior. After the fizzing was stopped, the vial was sealed for 30 min to reach equilibrium in 2-mercaptobenzothiazole distribution. The halloysite suspension was centrifuged to remove excess dissolved 2-mercaptobenzothiazole, cleaned in water three times, and dried. This process was repeated four times to ensure the saturation of the inner halloysite cavity with precipitated 2-mercaptobenzothiazole. During the first three cycles, the loading of 2-mercaptobenzothiazole into halloysites was increased gradually with the increment of 25 mg of 2-mercaptobenzothiazole per 1 g of the halloysite. The saturation loading level was achieved after the fourth loading step. The maximum 2-mercaptobenzothiazole quantity loaded into the halloysite tubes was 5 wt %

Thus, loaded halloysite nanotubes have no defined release ability and entrapped 2-mercaptobenzothiazole can be released spontaneously because of its partial solubility in water. To attain controlled release properties to the halloysite nanotubes, we modified the surface of the nanotubes by layer-by-layer deposition of two polyelectrolyte bilayers (poly(styrene sulfonate)/poly(allylamine hydrochloride)) from corresponding 2 mg/mL

polyelectrolyte solutions, so the openings at the edges became blocked with polyelectrolytes. The incubation time was 15 min; positive polyelectrolyte formed the first polyelectrolyte layer on the negatively charged halloysite surface (Figure 2). After adsorption of every polyelectrolyte layer, the halloysite material was washed with water by centrifugation in order to remove nonadsorbed polyelectrolyte molecules.

The ζ potential of the initial halloysite nanotubes is negative (Figure 2). Electrophoretic measurements indicate the charging of the nanotubes coated with the adsorbed polyelectrolyte layer upon each added layer. Figure 2 shows a drastic increase of the surface charge after deposition of the first PAH layer (+70 mV) followed by a similar (−82 mV) decrease after PSS adsorption on the next stage. The final nanocontainers have an inhibitor/halloysite/PAH/PSS/PAH/PSS layer structure. The SEM image of halloysites doped with 2-mercaptobenzothiazole and coated with polyelectrolytes layers is presented in Figure 3. Polyelectrolyte-coated halloysite material is composed of well-defined single tubes 100−300 nm thick as well as fractured small pieces of nanotubes. The polyelectrolyte shell attains controlled release properties to the halloysite nanotubes. The opening of the shell can be induced only by changing the surrounding pH value to the acidic or alkali region (which happens when the corrosion starts)[6] while in neutral pH the polyelectrolyte shell remains intact, preventing undesirable leakage of the entrapped inhibitor.

The release of the entrapped inhibitor into water at neutral and alkali pH is represented in Figure 4. Approximately 10% of the loaded material is released from halloysite nanotubes without polyelectrolyte shells after 6 days of storage in neutral water, so pure 2-mercaptobenzothiazole-filled halloysite cannot be directly applied in self-healing anticorrosion coatings. On the contrary, polyelectrolyte shells terminate the spontaneous release of the 2-mercaptobenzothiazole at neutral pH blocking the permeability of the halloysite nanotubes. Polyelectrolyte shells made of weak polycations (polyallylamine) and strong polyanions (polystyrene sulfonate) can be opened by increasing the pH value because of the formation of the defects between polyelectrolyte multilayers.[6] As seen from Figure 4, the release of the 2-mercaptobenzothiazole from halloysite nanotubes with polyelectrolyte shells is triggered at pH 10, similar to the pH value during the localized corrosion process. Thus, modification of halloysite nanotubes with polyelectrolyte shells is an important issue to achieve controlled release of the encapsulated inhibitor as well as to prevent its undesirable leakage from the coating.

3.2. Characterization of the Coatings. The properties of TPOZ/GPTMS-based sol−gel coatings, which are under study as an environmental friendly pretreatment for aluminum, are reported in our previous papers.[7,8,28,29] The sol−gel solution before application on metallic substrates is homogeneous, transparent, and has a light-yellow color. The viscosity of the hybrid mixed sols remains in the range of 12−35 cP within 1 month.[7] The high-resolution TEM image of the sol−gel coating applied on an aluminum-based substrate is presented in Figure 5. The TEM image of the cured hybrid coating shows that the film contains uniform amorphous nanoparticles enriched with zirconium, which are distributed homogeneously in the organosiloxane-based matrix. The nanoparticles were formed in situ during hydrolysis of TPOZ and have diameters of about 4 nm.

SEM images (Figure 6) show the plane view (a) and cross-section representation (b) of a halloysite-doped sol−gel film applied on an aluminum alloy. Halloysites disposed in different ways are visible on the surface of the sol−gel coatings. Neither cracks nor other defects induced by the addition of halloysites

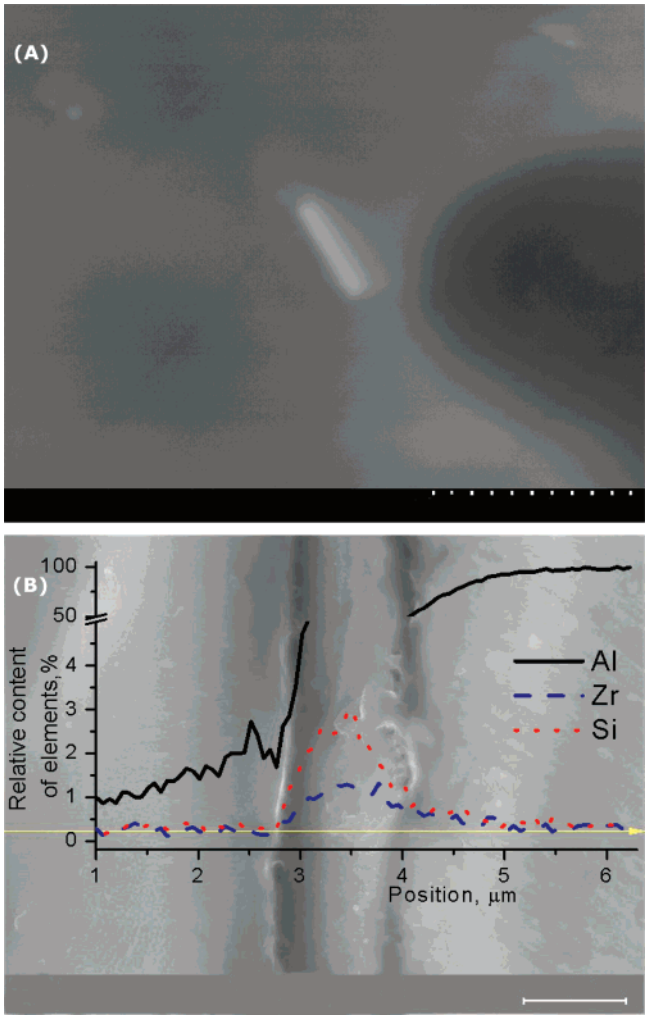

Figure 6. (a) SEM image of an AA2024 aluminum alloy coated by a sol−gel film doped with halloysites. Scale bar is 3.75 μm. (b) Cross-section image and EDX profile (along yellow arrow) of the same sol−gel film deposited on an AA2024 aluminum alloy. Scale bar is 1 μm.

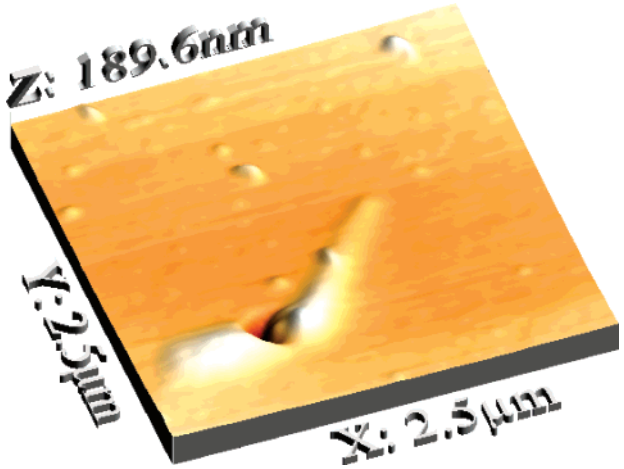

Figure 7. Topography image of sol−gel coating doped with halloysites.

were visualized on the surface with 8000 times magnification. The thickness of the sol−gel is around 1.0−1.2 μm. Figure 7 presents the AFM topography scan taken before the immersion of aluminum with an inhibitor-doped sol−gel coating into sodium chloride solution. Halloysites are distributed in the sol−gel coating without aggregation or accumulation on the surface of the film or on the coating−metal interface.

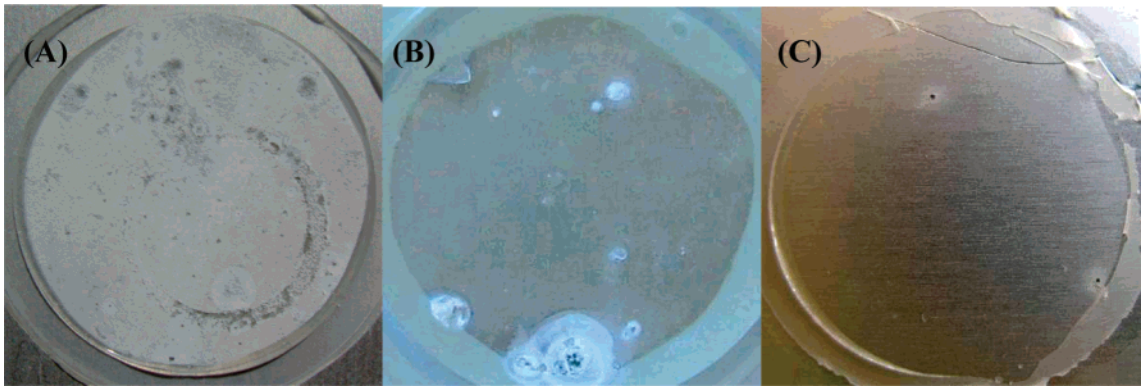

Figure 8. Optical photos of blank and differently treated AA2024 aluminum alloys. The pictures of all samples were taken after a 2-week immersion test in corrosive medium: (a) blank aluminum alloy immersed in 0.3% NaCl, (b) blank aluminum alloy immersed in 0.3% NaCl saturated with 2-mercaptobenzothiazole, and (c) aluminum alloy coated with halloysite-doped sol−gel film after immersion in 3% NaCl solution.

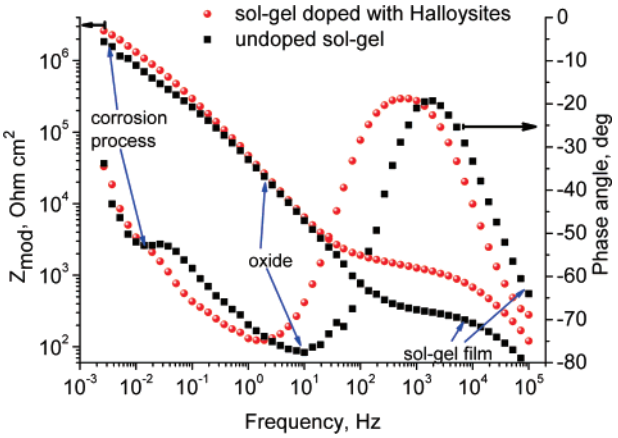

Figure 9. Impedance spectra of undoped and halloysite doped sol−gel coatings after a 2-week immersion test in 3% NaCl.

3.3. Corrosion Protection Performance. Figure 8 presents optical photos of the blank aluminum alloy (a and b) and an alloy panel coated with halloysite doped sol−gel film (c). Visual observation of the surface of the samples after 2 weeks of immersion in the corrosion medium demonstrates that the noncoated aluminum sample immersed in pure aqueous sodium chloride solution has many pits on the surface and is completely corroded. Addition of 2-mercaptobenzothiazole in solution (Figure 8b) decreases the number of pits and reduces the degree of corrosion attack.[30,31] However, the sample is still corroded after immersion in diluted NaCl solution (0.3%). The specimen coated with a thin sol−gel film doped by 2-mercaptobenzothiazole-loaded halloysites and immersed in 10 times more concentrated chloride electrolyte (3% NaCl solution) demonstrates a drastic decrease of corrosion attack (Figure 8c). The surface of that sample is visually almost intact and has only two small pits after such a long immersion test in a more aggressive electrolyte as compared to previous cases.

The main idea of introduction of halloysites into sol−gel coatings is the reinforcement of corrosion protection. EIS was used in this work to quantify the corrosion protection of different sol−gel films. EIS is one of the most intensively used and powerful techniques for investigation of corrosion protection.[32,33] The frequency dependence of the complex impedance of the coated substrate allows effective evaluation of the different components of the system such as capacitance and resistance of the protective layers, charge-transfer resistance, and double-layer capacitance, which are related to electrochemical corrosion activity. Figure 8 presents the impedance spectra of the AA2024 alloy samples coated with blank sol−gel films or sol−gel layers doped with halloysites. The spectra were taken after 2 weeks of accelerated immersion test in 3% NaCl solution. Three well-defined time constants appear in the spectrum of undoped sol−gel: the high-frequency one at about 100 kHz is related to the capacitance of the sol−gel coating, the second one at 10 Hz can be ascribed to the presence of an intermediate oxide layer on the metal surface, and the third time constant is related to the double-layer capacitance.[8,34] Although both coatings provide effective corrosion protection, the one with halloysites demonstrates half an order of magnitude better barrier properties of the sol−gel matrix and higher low-frequency impedance that reflects better corrosion protection performance.[34] The not well-defined character of the low-frequency time constant in the case of the AA2024 alloy substrate coated with the halloysite-doped sol−gel film also testifies the lower corrosion activity and consequently better corrosion protection.

The higher corrosion protection of sol−gel containing 2-mercaptobenzothiazole-doped halloysites can be explained by the inhibiting action of 2-mercaptobenzothiazole, which is the effective inhibitor for corrosion of aluminum alloys.[30] The function of inhibitor-doped halloysites is to keep and provide slow release of the inhibitor blocking the initial corrosion processes and healing microdefects in the coating. The halloysite-based nanocontainers prevent interaction of the inhibitor with components of the sol−gel matrix during the synthesis and, thereby, deactivation of inhibitor.

Conclusions

In conclusion, we demonstrated the applicability of commercially available and cheap nanotubes—halloysites in a new generation of anticorrosion coatings based on inhibitor-loaded nanocontainers. Halloysite nanotubes act as a reservoirs for inhibitor molecules, preventing their direct interaction with the coating matrix and undesirable leakage. Polyelectrolyte multilayers around the halloysite nanotubes provide effective storage and prolonged release of the inhibitor (2-mercaptobenzothiazole) "on demand" in the damaged zones. The release of the encapsulated inhibitor is regulated by pH changes in local corrosion areas because of the sensitivity of polyelectrolyte multilayers to changes in the surrounding environment. In addition, the demonstrated application of halloysite nanotubes may be used in the fabrication of coatings with several active functionalities (e.g., self-healing and antistatic) when several types of halloysites loaded with the corresponding active agent will be incorporated simultaneously into a coating matrix. This will surely be a matter of future intense research, which, as a result, could lead to a new generation of highly sophisticated multifunctional coatings.

Acknowledgment. The research was supported by DAAD/GRICES Germany/Portugal collaboration project (D/06/12931). S.V.L., M.L.Z., and K.A.Y. gratefully acknowledge their personal FCT (Portuguese Fundação para a Ciência e Tecnologia) grants SFRH/BPD/20537/2004, SFRH/BPD/26481/2006, and SFRH/BD/25469/2005. D.S. acknowledges the NanoFutur program of the German Ministry for Education and Research (BMBF). We thank Prof. Yuri Lvov, Louisiana Tech University, Ruston, for providing halloysite nanotubes and Prof. L. F. Dick and C. Trindade from Rio Grande do Sul Federal University, Porto Alegre, Brazil for the high-resolution TEM images of sol−gel coatings.

References and Notes

(1) Brooman, E. W. *Metal Finishing* **2002**, *100*, 48−53.
(2) Brooman, E. W. *Metal Finishing* **2002**, *100*, 42−54.
(3) Osborne, J. H. *Prog. Org. Coatings* **2001**, *41*, 280−286.
(4) Twite, R. L.; Bierwagen, G. P. *Prog. Org. Coatings* **1998**, *33*, 91−100.
(5) Garcia-Heras, M.; Jimenez-Morales, A.; Casal, B.; Galvan, J. C.; Radzki, S.; Villegas, M. A. *J. Alloys Compd.* **2004**, *380*, 219−224.
(6) Shchukin, D.; Möhwald, H. *Adv. Funct. Mater.* **2007**, *17*, 1451−1458.
(7) Shchukin, D.; Zheludkevich, M.; Yasakau, K.; Lamaka, S.; Ferreira, M. G. S.; Möhwald, H. *Adv. Mater.* **2006**, *18*, 1672−1678.
(8) Zheludkevich, M. L.; Shchukin, D. G.; Yasakau, K. A.; Möhwald, H.; Ferreira, M. G. S. *Chem. Mater.* **2007**, *19*, 402−411.
(9) Abu, Y. M.; Aoki, K. *J. Electroanal. Chem.* **2005**, *583*, 133−139.
(10) Tomalino, M.; Bianchini, G. *Prog. Org. Coatings* **1997**, *32*, 17−24.
(11) White, S. R.; Sottos, N. R.; Geubelle, P. H.; Moore, J. S.; Kessler, M. R.; Sriram, S. R.; Brown, E. N.; Viswanathan, S. *Nature* **2001**, *409*, 794−797.
(12) Cho, S. H.; Andersson, H. M.; White, S. R.; Sottos, N. R.; Braun, P. V. *Adv. Mater.* **2006**, *18*, 997−1000.
(13) Schmidt, C. Anti-corrosive Coating Including a Filler with a Hollow Cellular Structure. U.S. Patent 6,383,271, May 7, 2002.
(14) Lammerschop, O.; Roth, M. Silikatische Partikel. German Patent DE 10064638 A1, July 4, 2002.
(15) Sutherland, W. M. Method for Protecting Surfaces against Environmental Damage and the Resultant Products. U.S. Patent 3,899,624, August 12, 1975.
(16) Veerabadran, N.; Price, R.; Lvov, Y. *Nano J.* **2007**, *2*, 531−535.
(17) Shchukin, D.; Sukhorukov, G. B.; Price, R.; Lvov, Y. *Small* **2005**, *1*, 510−513.
(18) Lvov, Y.; Price, R.; Gaber, B.; Ichinose, I. *Colloids Surf., A* **2002**, *198*, 375−382.
(19) Kommireddy, D.; Sriram, S.; Lvov, Y.; Mill, D. *Biomaterials* **2006**, *27*, 4296−4303.
(20) Singh, B.; Gilkes, R. *Clays Clay Miner.* **1992**, *40*, 212−215.
(21) Levis, S. R.; Deasy, P. B. *Int. J. Pharm.* **2002**, *243*, 125−134.
(22) Baral, S.; Brandow, S.; Gaber, B. *J. Am. Chem. Soc.* **1994**, *116*, 29.
(23) Yang, L.; Fassihi, R. *Int. J. Pharm.* **1997**, *155*, 219−229.
(24) Price, R.; Gaber, B.; Lvov, Y. *J. Microencapsulation* **2001**, *17*, 713−717.
(25) Luca, V.; Thomson, S. *J. Mater. Chem.* **2000**, *10*, 2121−2127.
(26) Chandler, H. M.; Healy, K.; McGregor, A.; Premier, R. R.; Hurrell, J. G. R. *J. Immunol. Meth.* **1982**, *53*, 187−194.
(27) MatWeb: Material Property Data (http://www.matweb.com/).
(28) Lamaka, S. V.; Zheludkevich, M. L.; Yasakau, K. A.; Montemor, M. F.; Cecilio, P.; Ferreira, M. G. S. *Electrochem. Commun.* **2006**, *8*, 421−428.
(29) Lamaka, S. V.; Zheludkevich, M. L.; Yasakau, K. A.; Serra, R.; Poznyak, S. K.; Ferreira, M. G. S. *Prog. Org. Coatings* **2007**, *58*, 127−135.
(30) Zheludkevich, M. L.; Yasakau, K. A.; Poznyak, S. K.; Ferreira, M. G. S. *Corros. Sci.* **2005**, *47*, 3368−3383.
(31) Lamaka, S. V.; Zheludkevich, M. L.; Yasakau, K. A.; Montemor, M. F.; Ferreira, M. G. S. *Electrochim. Acta* **2007**, *52*, 7231−7247.
(32) Macdonald, D. D.; McKubre, M. C. H. in *Impedance Spectroscopy Theory, Experiment, and Applications;* Barsoukov, E., Macdonald, J. R., Eds.; John Wiley & Sons, Inc.: Hoboken, NJ, 2005; pp 343-429.
(33) Borona, P. L.; Deflorian, F.; Fedrizzi, L. *Electrochim. Acta* **1996**, *41*, 1073−1082.
(34) Zheludkevich, M. L.; Serra, R.; Montemor, M. F.; Yasakau, K. A.; Salvado, I. M. M.; Ferreira, M. G. S. *Electrochim. Acta* **2005**, *51*, 208−217.